Chapter

Analysis of the Absorption Phenomenon through the Use of Finite Element Method

Minerva Robles-Agudo, Martha Patricia Gonzalez-Tejeda, Porfirio Esau Martinez-Muñoz and Ignacio Rojas-Rodríguez

Abstract

In this text, a numerical model using the finite element method (FEM) is developed to describe absorption phenomena using the Beer–Lambert law. Numerical results are compared against experimental measurements made on alpha brass, characterized by photothermal radiometry (PTR). Results from the numerical analysis are in good agreement with the measurements obtained from the radiometry tests. In this technique the material is subjected to a laser heating, producing a thermal wave that is captured with a detector by means of the amplitude and phase parameters. The analysis of the data obtained from six samples provides information about their thermal properties, such as conductivity and diffusivity, which can be correlated with structural changes in a material. Results from this research lead to the characterization of mechanical properties of metallic materials.

Keywords: light absorption, Beer–Lambert law, photothermal radiometry, finite element method

1. Introduction

Applications of materials in the industry depend on their physical–chemical properties. Metal and semiconductor materials have had a big relevance for humanity development, facilitating the life and making possible technological advances still today. The properties and characteristics of metals are taken into account for the selection of materials according to the function we will perform.

Copper alloys are materials known for a wide range of applications. Currently more than 400 copper alloys are known, among which brass and bronze are distinguished. It is possible to vary the amounts of copper and zinc in these alloys to obtain a variety of brass with different properties [1, 2].

Brass is considered one of the most important copper alloys due to the amount of zinc that can be varied considerably, ranging between 5 and 45% by weight. It is possible to produce a wide variety of brass alloys with different technological properties for various commercial and industrial applications. Among the most commonly used brass in engineering areas is high-strength brass, suitable for heavy loads, with adequate properties to resist wear and corrosion. Among the main advantages of these materials are their mechanical properties by thermal treatment and their low cost [3–5].

In 2010 Ozgowiez et al. [6] analyzed the influence of recrystallization annealing temperature on the microstructure and mechanical properties of Cu 30% Zn brass, which was subjected to cold deformation with a variable tension in the rolling process. The mechanical test showed that the properties of the brass deteriorated and the properties of the plastic increased as the recrystallization temperature increased within the range of 400–650°C [7].

In 1967 Bailey studied the structure and strength of an alpha brass with 20%$_w$ Zn, 6%$_w$ Ni, and 1.5%$_w$ Al. Brass samples were subjected to solution heat treatment (SHT) at 800°C for 2 h followed by quenching with water. Subsequently, the samples were thermally treated for 2 h at 300, 400, 500, 600, and 700°C. The best mechanical properties were obtained at 500°C PHT temperature [8].

Infrared photothermal radiometry (PTR) is an optical technique used for the characterization of metallic materials such as brass, to determine the influence of the precipitation heat treatment (PHT) temperature on metallurgical microstructure, thermal properties, and microhardness. This technique is based in light absorption and consists of a laser beam incident on a sample, which will absorb the radiation and emit a thermal wave that is detected by an infrared sensor. The signals of thermal wave are translated as amplitude and phase parameters. Compared with other characterization techniques, this technique has no destructive properties and has the advantage of not having direct contact with the sample to be analyzed.

One of the most important aspects to consider in the PTR is the process of light absorption in the material to be analyzed. As trivial as this may sound, absorption very often turns out to be the most critical and cumbersome step in laser processing. An enormous amount of work has been dedicated to investigating laser absorption mechanisms under various circumstances, and a great deal can be learned from this work for the benefit of laser-material processing.

Absorption process can be thought of as secondary "source" of energy inside the material. While driven by the incident beam, it tends to develop its own dynamics and can behave in ways deviating from the laws or ordinary optics. It is this "secondary" source, rather than the beam emitted by the laser device, which determines what happens to the irradiated material [9].

Certain wavelengths of light can be selectively absorbed by a substance or a material according to its molecular structure. The absorption of light occurs when an incident photon promotes the transition of an electron from a state of lower to higher energy. Excited electrons eventually lose this gained energy, and by a spontaneous radiation process, they return to their initial state.

The radiation emitted by a molecule, or an atom, after it has absorbed energy to place itself in an excited state, is defined as luminescence, depending on the nature of the excited state. All spectrophotometric methods are based on two laws that combined which are known as Beer–Lambert law. This law states that the light absorbed by a semitransparent medium is independent of the intensity of incident light, and each successive layer of the medium absorbs an equal fraction of the light passing through it. This amount of light can be calculated by Eq. (1), where I_0 is the incident light intensity, I is the transmitted light intensity, l is the length through which the light passes in the spectrophotometer cell, and k is the constant of the medium:

$$\log\left(\frac{I_0}{I}\right) = kl \tag{1}$$

In the absorption spectrometry, the comparison of incident light intensity before and after the interaction with a sample can be carried out nowadays, by means of different software. In the development of theoretical models, it is possible to include

properties of the materials and parameters that describe the process system, such as the direction or directions of the incidence of light and wavelength, among others.

Finite element method (FEM) is one of the most practical methods for solving engineering problems. This general numerical method is used to approximate solutions of partial differential equations very complicated in the resolution of problems that involve a high degree of mathematical and physical–mathematical performance. FEM is applied to character geometries and multiphysical behavior, both of material properties and of problems where it is generally not possible to obtain any analytical solution directly with the use of mathematical expressions. Some of the areas that use the finite element method to solve problems are heat transfer, fluid flow, mass transport, distribution of electromagnetic fields, and structural analysis, among others.

FEM allows obtaining an approximate numerical solution on a body, structure, or domain (continuous medium). On this domain certain differential equations are defined in an integral form that characterizes the physical behavior of the problem, dividing it into a high number of non-subdomains intersecting each other called "finite elements." This set of finite elements forms a partition of the domain also called discretization. Within each element there are a series of representative points called nodes. Two nodes are adjacent if they belong to the same finite element; in addition, a node on the edge of a finite element can belong to several elements. The set of nodes considering their adjacency relationships is called "mesh."

Calculations are carried out on this mesh of points called nodes, which serve as the basis for the discretization of the domain in finite elements. The creation of the mesh is done in a stage prior to the calculations called pre/process and usually with special programs called mesh generators. According to these adjacency or connectivity relations, the value of a set of unknown variables defined in each node and called degrees of freedom is related. The set of relations between the values of a given variable between the nodes can be written as a system of linear (or linearized) equations. The matrix of the said system of equations is called the system's stiffness matrix. The number of equations of said system is proportional to the number of nodes.

The FEM is widely used due to its generality and the ease of introducing complex calculation domains (in two or three dimensions). In addition, the method is easily adaptable to problems of heat transmission, fluid mechanics to calculate fields of velocities and pressures (computational fluid mechanics, CFD), or electromagnetic field. Given the practical impossibility of finding the analytical solution to these problems, often in engineering practice, numerical methods and, in particular, finite elements become the only practical alternative to calculation. One important property of the method is convergence; if finite element partitions are considered successively finer, the calculated numerical solution converges rapidly toward the exact solution of the system of equations.

For all the above, the FEM is an excellent method to consider the development of theoretical models for the analysis of the phenomenon of the absorption of radiation in materials. In this chapter, an analysis of absorption process as result of laser-material interactions using Beer–Lambert law is shown. In Section 2.1 a model absorption using COMSOL Multiphysics with finite element method in alpha brass is described. In Section 3 experimental results of photothermal radiometry technique applied to alpha brass are shown.

2. Analysis of laser-material interactions using Beer–Lambert law

When a light beam incident upon a semitransparent material, part of the energy supplied by it will be absorbed by the material. This process can be described through Beer–Lambert law. If we consider monochromatic and collimated light,

such as laser light, and we despise losses by reflection and dispersion in the material, considering a minimum refraction and scattering, the Beer–Lambert law can be written in differential form for the light intensity **I** as

$$\frac{\partial \boldsymbol{I}}{\partial z} = \alpha(T)\boldsymbol{I} \tag{2}$$

where z is the coordinate along the beam direction and $\alpha(T)$ is the temperature-dependent absorption coefficient of the material. Because the temperature can vary in space and time, we must also solve the next governing partial differential equation for temperature distribution within the material:

$$\rho C_p \frac{\partial T}{\partial t} - \nabla \cdot (k \nabla \mathrm{T}) = \mathrm{Q} = \alpha(T)\boldsymbol{I} \tag{3}$$

where Q is the heat source term equals the absorbed light. Eqs. (2) and (3) present a bidirectionally coupled multiphysics problem that is possible to solve within the core architecture of COMSOL Multiphysics program based in the finite element method [10].

2.1 Beer–Lambert law deviations

Beer–Lambert law states that the optical density is directly proportional to the concentration of the species they absorb. However, deviations from this law can occur due to instrumental and intrinsic causes [11–13]. Among the main deviations from Beer–Lambert law are the following:

2.1.1 Light scattering

There are two dispersion phenomena, one depends on the size of the solute particle or any suspended material. Biological samples are usually cloudy because macromolecules or other large aggregates scatter light. The optical densities resulting from the scattering of light are proportional to $1/\lambda^4$ (Rayleigh scattering) and can therefore be recognized as an absorption background which increases rapidly with the decrease in wavelength [14]. The second type of dispersion is known as the Raman scattering. In this phenomenon, part of the excitation energy of light is abstracted by vibrational modes of the solvent molecules. In the case of water or hydroxyl solvents, the most dominant vibrations that absorb this energy are the OH groups, whose vibration energy is observed at a wavelength of 3300 cm^{-1}. The Raman signal of the solvents will be observed at a wavelength that is 3300 cm^{-1} less in energy than the excitation wavelength. The wavelength of the Raman scattering (λ_{RA}) can be calculated as $\lambda_{RA}^{-1} = \lambda_{ex}^{-1} - 0.00033$ [15].

2.1.2 Fluorescence

If the optical density of the sample is high and if the absorbing species are fluorescent, the emitted light can reach the detector. This process will result in derivations of Beer–Lambert law. The effect can be minimized by maintaining the distance of the detector from the sample and decreasing the efficiency with which the emission fluorescence is collected.

2.2 Use of COMSOL multiphysics to model absorption in alpha brass through FEM

COMSOL Multiphysics is a general-purpose simulation software for modeling designs, devices, and processes in all fields of engineering, manufacturing, and

scientific research. The platform product can be used on its own or expanded with functionality from any combination of add-on modules for simulating electromagnetic fields, structural mechanics, acoustics, fluid flow, heat transfer, and chemical engineering. The add-on modules and LiveLink™ products connect seamlessly for a modeling workflow that remains the same regardless of what you are modeling.

Engineers and scientists use the COMSOL Multiphysics® software to simulate designs, devices, and processes in all fields of engineering, manufacturing, and scientific research. This simulation platform encompasses all of the steps in the modeling workflow—from defining geometries, material properties, and the physics that describe specific phenomena to solving and postprocessing models for producing accurate and trustworthy results [16].

In this section a simple model in COMSOL developed for the analysis of laser light absorption in alpha brass samples is described. The geometry of the problem is described using a concentric double cylinder, where the external cylinder represents the sample being heated, with a diameter of 40 mm, while the diameter of the internal cylinder represents the diameter of the laser beam, with a diameter of 10 mm, as shown in **Figure 1**. According to the geometry defined in the problem, a collimated beam with a constant intensity distribution is considered, in which the effects of divergence are neglected. In the general analysis, the domain is divided into two volumes, which are equivalent to the two cylinders. These volumes represent the same material, but only Beer–Lambert law is resolved in the internal domain (internal cylinder), which is the only region in which the material is heated by the laser beam. To implement Beer–Lambert law, it starts by adding the PDE interface with the dependent variables and unit settings.

The equation itself is implemented via the general form PDE interface. Aside from the source term, f, all terms within the equation are set to zero; thus, the equation being solved is $f = 0$. The source term is set to Iz-(50[1/m]*(1 + (T-300[K])/40[K]))*I, where the partial derivative of light intensity with respect to the z-direction is Iz, and the absorption coefficient is (50[1/m]*(1 + (T-300[K])/40[K])), which introduces temperature dependency for illustrative purposes. This one line implements the Beer–Lambert law for a material with a temperature-dependent absorption coefficient, assuming that it will also solve for the temperature field, T, in this model.

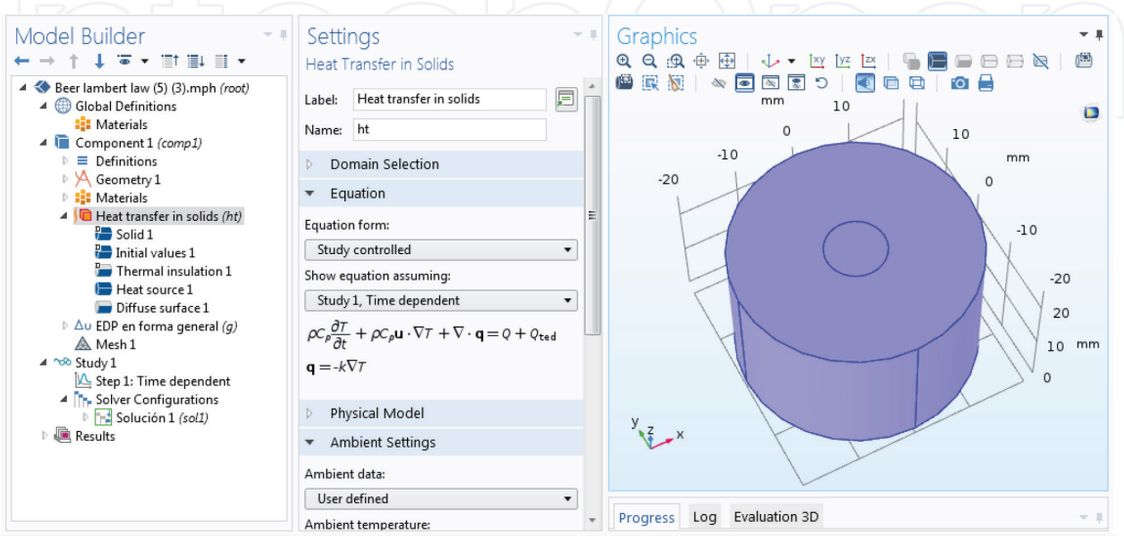

Figure 1.
Definition of the cylindrical geometry, parameters, and initial conditions for the absorption analysis model in alpha brass.

Since this equation is linear and stationary, the initial values do not affect the solution for the intensity variable. The zero-flux boundary condition is the natural boundary condition and does not impose a constraint or loading term. It is appropriate on most faces, with the exception of the illuminated face. We will assume that the incident laser light intensity follows a Gaussian distribution with respect to distance from the origin. At the origin, and immediately above the material, the incident intensity is 0.3 W/mm^2. Some of the laser light will be reflected at the dielectric interface, so the intensity of light at the surface of the material is reduced to 0.95 of the incident intensity. This condition is implemented with a Dirichlet boundary condition. At the face opposite to the incident face, the default zero-flux boundary condition can be physically interpreted as meaning that any light reaching that boundary will leave the domain.

With these settings described above, the problem of temperature-dependent light absorption governed by the Beer–Lambert law has been implemented. It is, of course, also necessary to solve for the temperature variation in the material over time. In this case thermal conductivity of alpha brass of 93.32 W/m/K is considered, with a density of 2000 kg/m^3 and a specific heat of 1000 J/kg/K that is initially at 300 K with a volumetric heat source.

The heat source itself is simply the absorption coefficient times the intensity or, equivalently, the derivative of the intensity with respect to the propagation direction. Most other boundaries can be left at the default thermal insulation, which will also be appropriate for implementing the symmetry of the temperature field. However, at the illuminated boundary, the temperature will rise significantly, and radiative heat loss can occur. This can be modeled with the diffuse surface boundary condition, which takes the ambient temperature of the surroundings and the surface emissivity as inputs.

It is worth noting that using the diffuse surface boundary condition implies that the object radiates as a gray body. However, the gray body assumption would imply that this material is opaque. So how is it possible to use Beer–Lambert law, which is appropriate for semitransparent materials? It is possible to solve this apparent discrepancy by observing that the absorption capacity of the material is highly dependent on the wavelength. The depth of penetration is relatively large. However, when the part is heated, it is reradiated mainly in the long infrared regime. At long infrared wavelengths, it is possible to assume that the depth of penetration is very small and, therefore, the assumption that the volume of the material is opaque for radiation is valid.

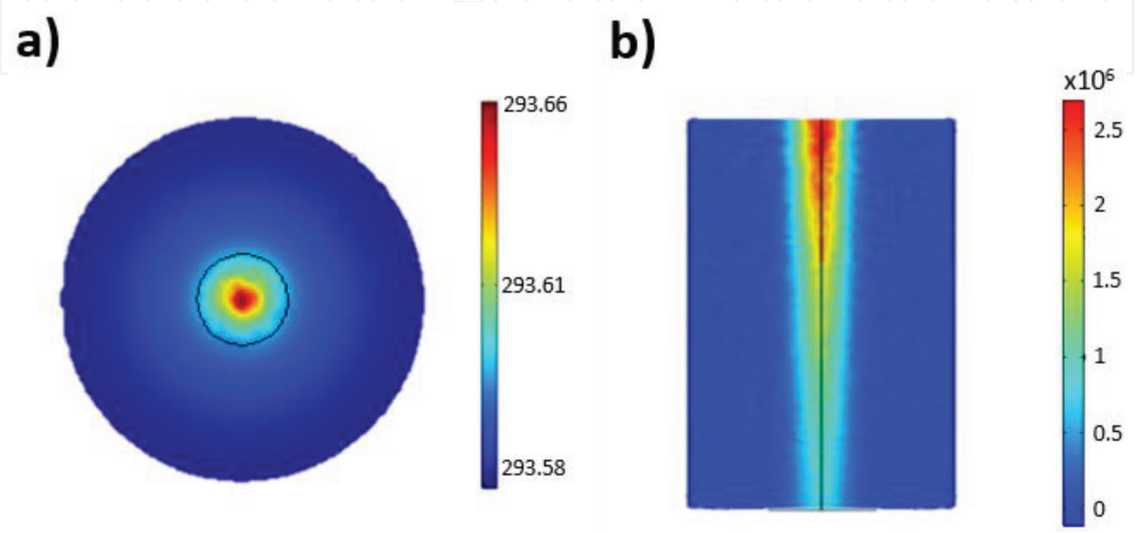

Figure 2.
Propagation of heat in the alpha brass material, (a) surface profile and (b) penetration profile.

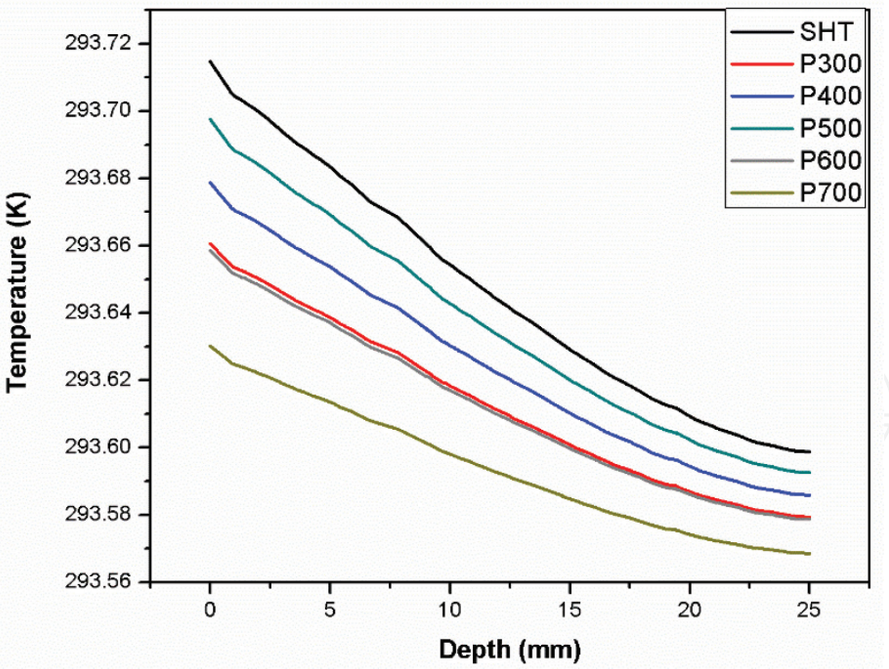

Figure 3.
Temperature as a function of depth along the centerline over 40 seconds of time, for six different samples of alpha brass.

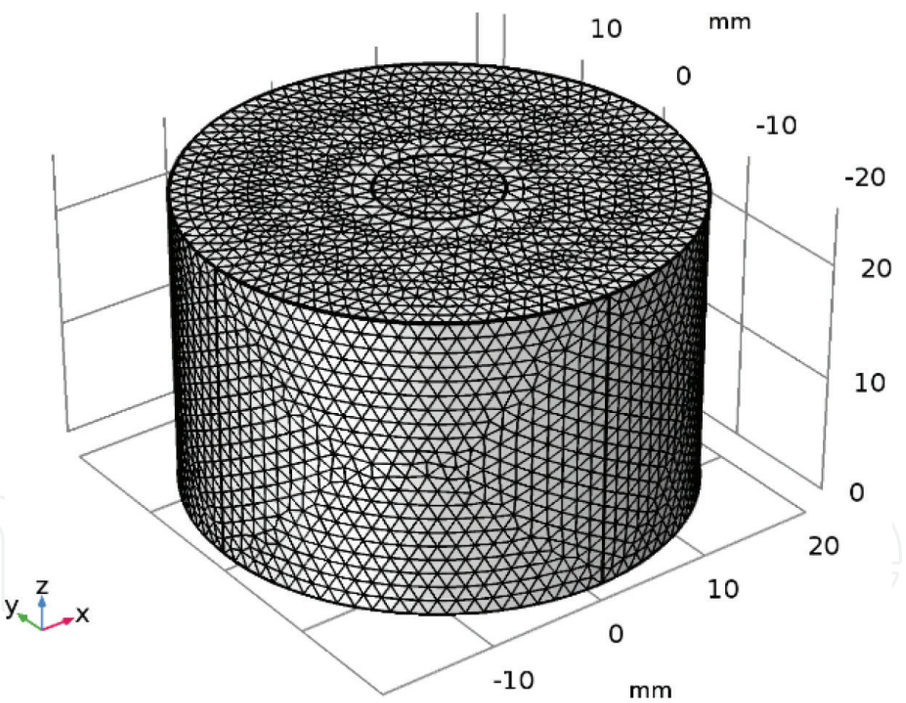

Figure 4.
Creation of the mesh for the calculation of the heat distribution in alpha brass by means of the finite element method.

It is possible to solve this model either for the steady-state solution or for the transient response. In **Figure 2** the propagation of heat in the alpha brass material is shown. In **Figure 3** the changes of temperature as a function of depth along the centerline over a time of 40 seconds for six different kinds of alpha brass are shown.

In **Figure 4** the mesh used to solve the equations through finite element is shown. Although it is not necessary to use a swept mesh in the absorption direction, applying this feature provides a smoot solution for the light intensity with relatively fewer elements than a tetrahedral mesh. The plot of temperature with respect to

depth at the centerline illustrates the effect of the varying absorption coefficient due to its increase.

3. Experimental methods to characterize Kunial alpha brass through thermal treatments

The Kunial alpha brass is a copper-zinc alloy plus nickel and corresponds to an alpha brass with chemical composition of 20% Zn_w, 6% Ni_w, 1.5% Al_w, and the balance Cu. Six samples were characterized; one of them with solution heat treatment (SHT), as reference. Where SHT is the heating of an alloy to a temperature at which a particular constituent will enter into solid solution followed by cooling at a rate fast enough to prevent the dissolved constituent from precipitating. The other five samples were treated at different precipitation heat treatment (PHT) temperatures, as shown in **Table 1**. The thermal treatment by precipitation involves the addition of impurity particles to increase the strength of a material. PHT Samples were metallographically prepared with 240, 320, 400, 600, and 1000 grit sandpapers. Then, specimens were polished with 0.3 μm alumina and etched with 2 g of $K_2Cr_2O_7$, 8 ml of H_2SO_4, 4 ml of NaCl saturated solution, and 100 ml of distilled H_2O.

To measure the hardness of the materials, 16 indentations were practiced on each polished brass sample, according to ASTM E92. One Leco Model LM300AT Vickers microhardness tester at 100 g load, according to ASTM-E70, was used [17]. The reported Vickers microhardness is shown in **Table 1**. Thermal diffusivity, conductivity, and heat capacity results of Kunial brass are shown in **Table 1**.

3.1 Thermal diffusivity

An open photoacoustic cell (OPC) was used to analyze the thermal diffusivity of samples [5]. Thicknesses and characteristics of samples are described in **Table 1**. In experimental setup the samples were placed on top of electret microphone, where a laser (450 nm wavelength) modulated was focused onto the sample surface. Frequency modulation range from 15 to 400 Hz was used. Photoacoustic technique was used to observe amplitude and phase signal behaviors in the sample [18, 19]. A thermal diffusion model was used to calculate the pressure at the photoacoustic gas

Sample	PHT temperature °C	Thickness (μm)	Vickers microhardness [8]	α (cm^2/s)	ρC (J/m^3-K)	k (W/m-K)	Vickers microhardness (PTR technique)
SHT	NA	387	72	0.242	3.49×10^6	84.46	83.7
P300	300	392	82	0.463	2.60×10^6	120.46	92.1
P400	400	375	140	0.415	2.55×10^6	105.44	121.2
P500	500	392	201	0.339	2.77×10^6	93.32	200.6
P600	600	398	162	0.508	2.42×10^6	122.42	154.2
P700	700	401	135	0.587	2.70×10^6	158.63	133.5

Table 1.
Thermal properties, Vickers microhardness, and thermal diffusivity of Kunial brass samples.

chamber [20], with the simplification for the thermally thick and optically opaque regime [21] according to the following equation:

$$V_{OPC} = \frac{A}{f} e^{-\sqrt{\frac{f}{f_c}}} \tag{4}$$

where A is a constant that contains geometric parameters including factors as gas thermal properties, light beam intensity, and room temperature, f is the frequency scan, and f_c is the cutoff which separates thick and thin regimens. The cutoff is related to thermal diffusivity α and the sample thickness l by the following equation [21]:

$$\alpha = \pi l^2 f_c \tag{5}$$

3.2 Heat capacity

The thermal relaxation method was used to determine the heat capacity [8]. In the experimental setup, a thermocouple was connected to the back side of the sample. A laser light source of 450 nm wavelength was focused onto the sample surface with a continuous incidence and uniformly. Conduction and convection energy losses were reduced by a vacuum disposal, thereby mainly ensuring a radiation heat transfer [22]. The temperature variation was determined by

$$\Delta T(t) = \frac{P_0}{\eta}\left(1 - e^{-\tau/T}\right) \tag{6}$$

where τ value is related to the heat capacity by

$$\rho C_p = \frac{8\varepsilon\sigma T_0^3}{l_m} \tag{7}$$

and ε is the thermal emissivity, considered 1 in this case, and σ is the Stefan Boltzmann constant. T_0 is the temperature, and l_m is the thickness. The thermal conductivity is related to the heat capacity and thermal diffusivity by

$$k = \alpha\rho C_p \tag{8}$$

3.3 Photothermal radiometry (PTR)

Figure 5 shows the principle of PTR, where a beam of laser light is focused on a material. The radiation absorbed by the material penetrates a certain depth and becomes a wave of heat which propagates through the material. Using an infrared detector, it is possible to detect the signals coming from the thermal wave translated in amplitude and phase. In **Figure 6** the experimental setup of photothermal radiometry technique is shown. PTR technique was used to obtain thermal images of alpha brass samples. A high-power semiconductor laser (450 nm wavelength, 300 mW) was used. The laser beam was collimated, and then it was focused onto the surface of the sample with a 40 μm spot size using a GRADIUM lens. The modulated infrared radiation from the excited surface was collected and collimated by two off-axis paraboloid mirrors, and then, it was focused onto a Judson Model J15D12-M204 HgCdTe detector, which was cooled by liquid nitrogen. The detector signal was amplified by a low-noise preamplifier, and then, it was sent to a lock-in amplifier SRS-850 which was interfaced

with a PC. XYZ microstages were used to obtain PTR amplitude and phase images [23, 24].

An area of 2×2 mm in each sample was scanned to obtain the thermal images. The PTR technique comprises the optical excitation of the sample with a modulated laser light source and the detection of the recombination-induced infrared emission. PTR technique covers the thermal infrared emission band from 2 to 12 μm. In PTR the amplitude and phase signals parameters were obtained from a highly focused laser beam, with a waist of 40 μm.

The thermal wave generated in the sample becomes attenuated at a distance μ, thermal length. Only information due to changes in the thermal properties of the surface of the sample is obtained. The thermal length is defined by

$$\mu = \sqrt{\frac{\alpha}{\pi f}} \tag{9}$$

where α is the thermal diffusivity of the sample and $f = \omega/2\pi$.

The PTR amplitude signal generated in the sample due to the absorption of modulated laser can be described by the following equation (8):

$$T(x,t) = \frac{I_0}{2\varepsilon\sqrt{\omega}} exp\left(-\frac{x}{\mu}\right) cos\left(\omega t - \frac{x}{\mu} + \frac{\pi}{4}\right) \tag{10}$$

where ω is the angular frequency, I_0 is the laser intensity, x is the sample thickness, and ε is the thermal effusivity. The pre-factor in Eq. (10) is constant for a fixed modulation frequency $f = \omega/2\pi$.

The PTR amplitude signal is proportional to the reciprocal of the thermal effusivity, while the PTR phase lag is proportional to the x/μ term. The thermal effusivity and the thermal diffusivity are dependent parameters from the thermal wave propagation which determines the material inertia. The thermal effusivity is a significant heating periodic surface and a heat transport parameter. It is representing the dissipated heat energy in the solid material depending on the temperature change at the beginning of the periodic warming process. The thermal effusivity is related to Eq. (9) by the diffusivity coefficient (α), as shown in the following equation:

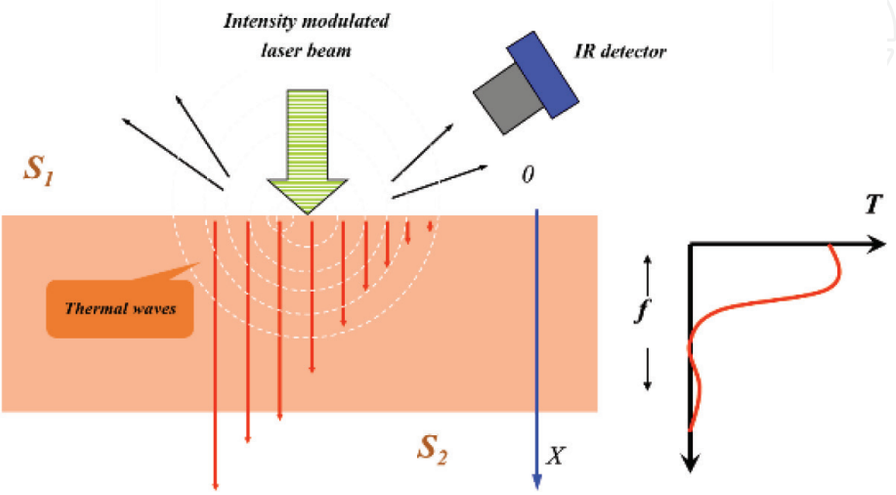

Figure 5.
Principle of PTR technique for characterization of a material.

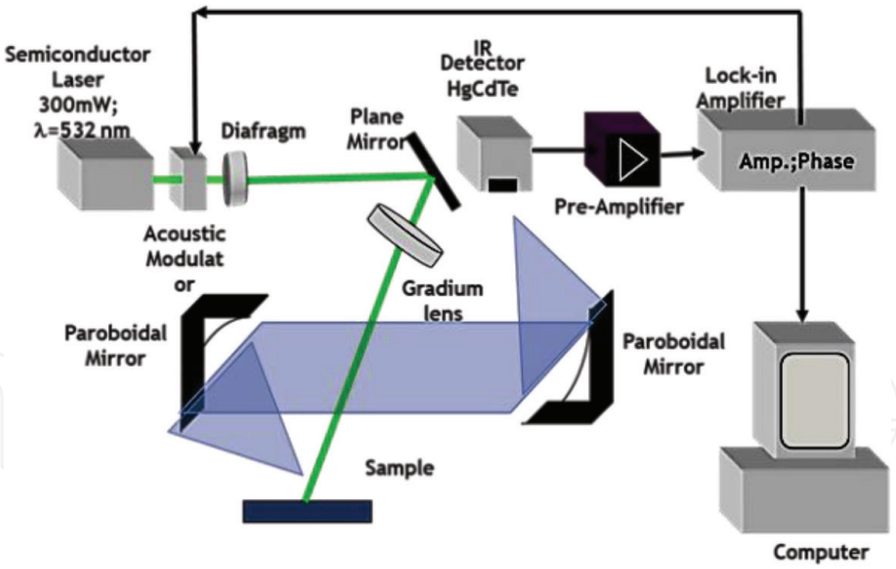

Figure 6.
Experimental setup of PTR technique.

$$\varepsilon = \frac{k}{\sqrt{\alpha}} = \sqrt{k\rho c} \tag{11}$$

where k is the thermal conductivity, ρ is the material density, and c is the specific heat at a constant volume.

3.4 Thermal properties

Lowest diffusivity and conductivity values that corresponded to the SHT sample are shown in **Figures 7a** and **b**. In **Figure 7c** the highest heat capacity value was for the SHT sample. The noticed behavior was that as diffusivity and conductivity increased, the heat capacity trended to decrease. This can be explained by the thermal treatment; due to the temperature increased, the grain size increased, and this had an effect on diffusivity and conductivity. The heat capacity decreased due to the PHT effect because intermetallic precipitates migrated to grain boundaries affecting the heat capacity.

3.5 Vickers microhardness and FWHM^{-1}

Vickers microhardness results are shown in **Figure 8a**. The lowest value of Vickers microhardness corresponds to the SHT sample and the highest value to the P500 sample. Due to recrystallization and precipitation phenomena, as the PHT temperature increased, the Vickers microhardness decreased. The precipitation had a little effect from 300 to 400°C. However, the P500 sample reached the highest Vickers microhardness value at 500°C. In P600 y P700 samples, the PHT temperature increased, and the microhardness decreased due to over aging.

In **Figure 8b** is shown that the FWHM^{-1} increased as the PHT temperature increased. As the Vickers microhardness decreased, the crystallinity quality increased. The lowest FWHM^{-1} value was at 400°C, and then, it trended to increase as the PHT temperature increased. The crystalline quality improved as the PHT temperature increased. In spite of the highest Vickers microhardness value being reached at 500°C (P500), higher temperatures caused that the Vickers

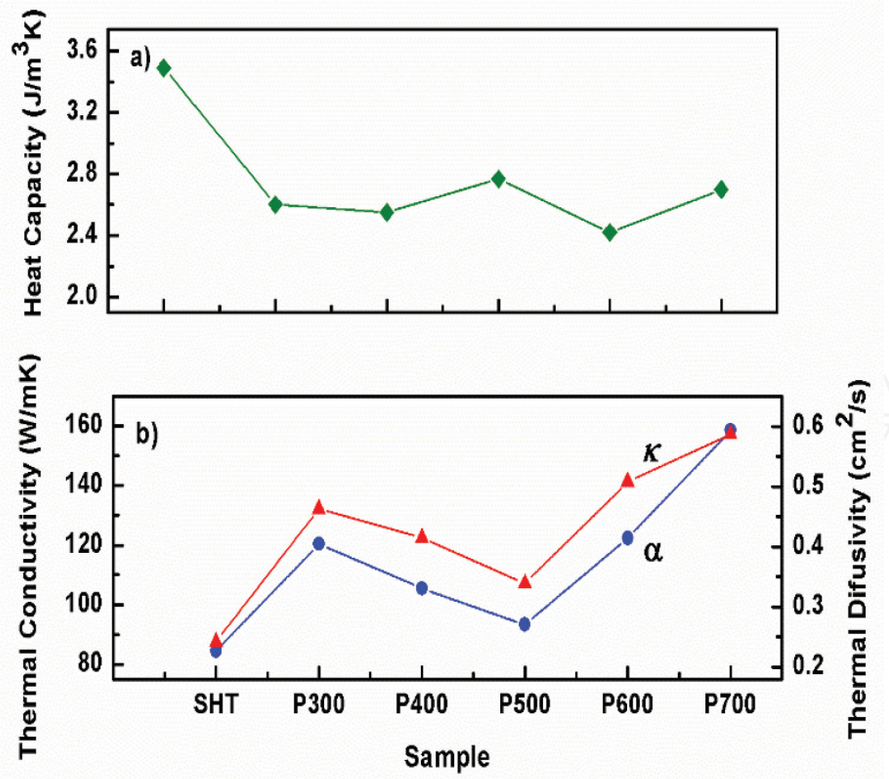

Figure 7.
Thermal properties of Kunial brass samples studied, (a) heat capacity and (b) diffusivity (κ) and conductivity (α).

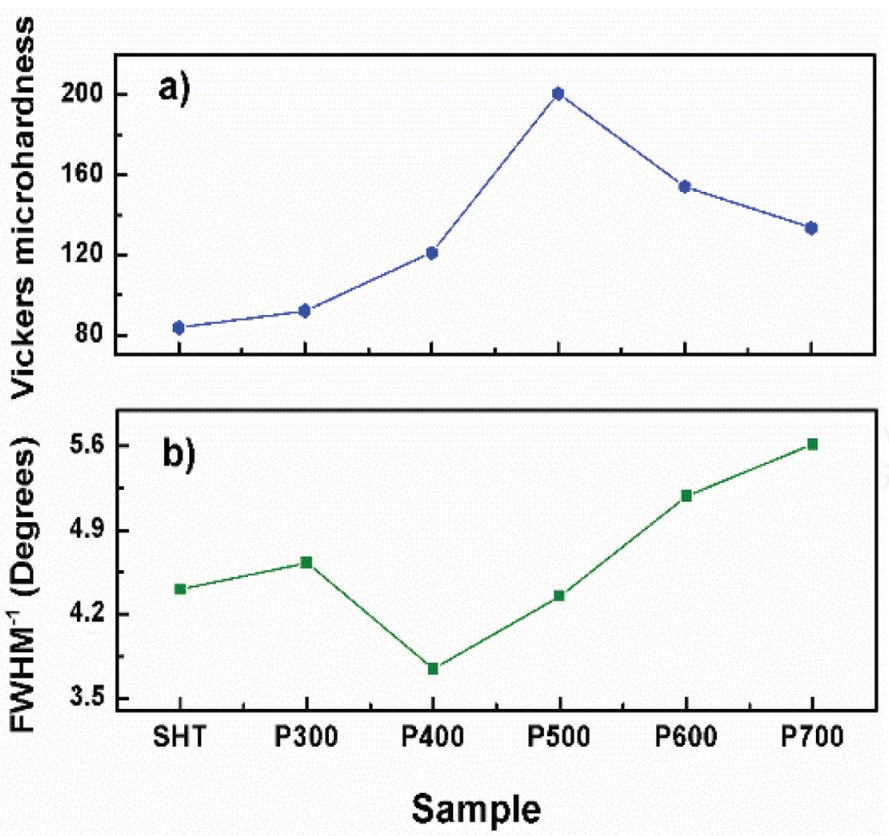

Figure 8.
(a) Vickers microhardness and (b) FWHM^{-1} of brass samples with different thermal properties.

microhardness trended to decrease. A result of a diffusive process at 600°C was observed due to the slow cooling temperature. These diffusive processes produced a recrystallization, improving the crystalline quality.

3.6 PTR images

In **Figure 9** PTR images are shown. In **Figure 9a**, it is shown that the amplitude increased as the PHT temperature increased until the highest signal of 500°C. Subsequently, amplitude signals decreased as the temperature increased until the lowest value of 700°C. However, no large phase signal changes were observed in **Figure 9b**.

The highest Vickers microhardness and the optimum precipitation were presented in the P500 sample. The lowest Vickers microhardness was obtained in the P700 sample. The comparison among the Vickers microhardness and PTR amplitude and phase signals is shown in **Figure 10**. Vickers microhardness trend is shown in **Figure 10a**. **Figure 10b** illustrates the amplitude behavior was similar to the hardness pattern, because the PTR signal was related to brass structural changes. The maximum PTR amplitude signal was reached at 500°C that is the optimum PHT temperature which corresponded to the maximum Vickers microhardness of the studied brass [25]. It is possible to observe in **Figure 10c**, that the phase signal

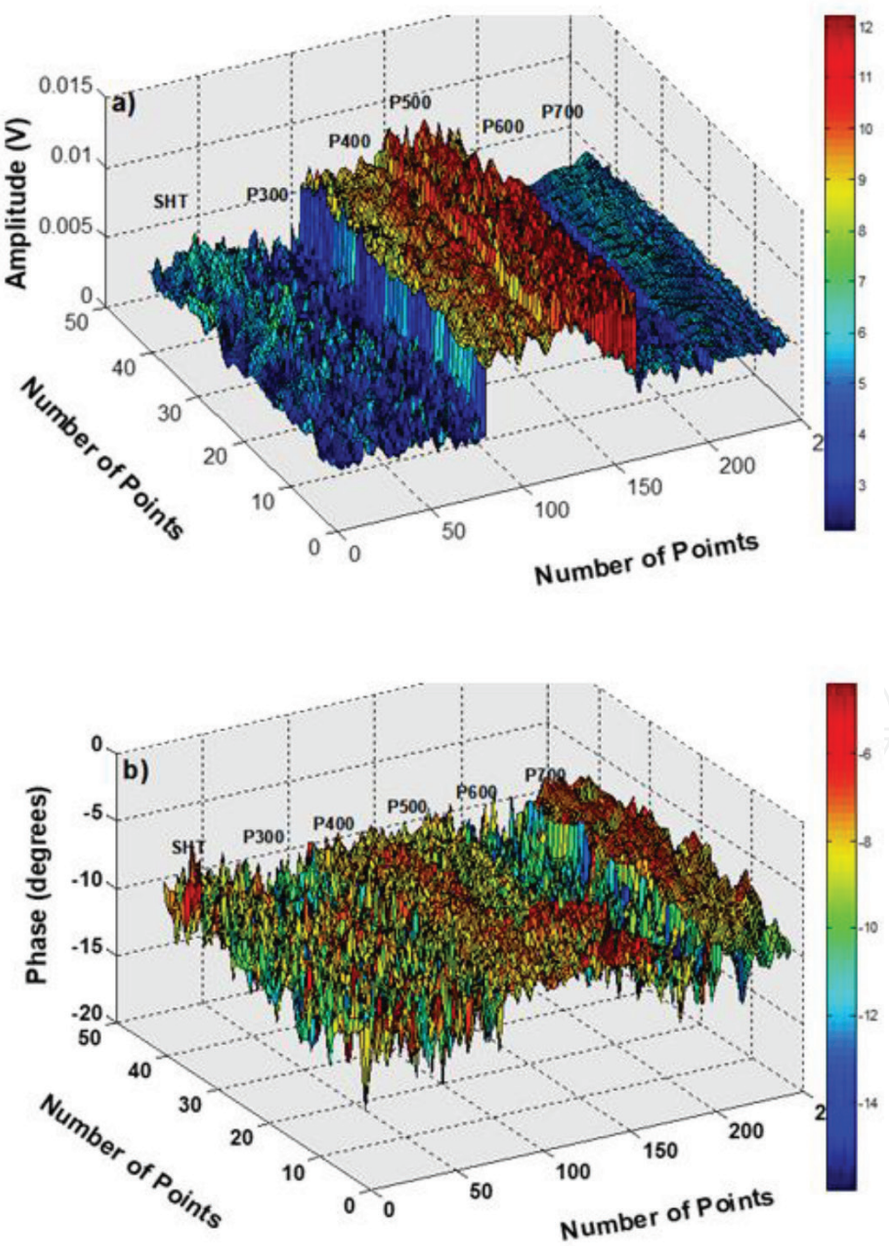

Figure 9.
Photothermal images experimental of brass samples, (a) amplitude and (b) phase.

behavior did not show large changes as in the amplitude signal. The highest PTR phase signal corresponded to the SHT sample, while the lowest PTR phase signal corresponded at 700°C. This means that the PTR amplitude signal was more sensitive than the PTR phase signal, to observe the effect of the PHT temperature on α brass thermal, structural, and Vickers microhardness properties.

4. Conclusions

The finite element method (FEM) offers an option for the solution of complex problems in engineering with a multiphysical profile and equations difficult to solve analytically. The model presented in this chapter, and developed on the COMSOL

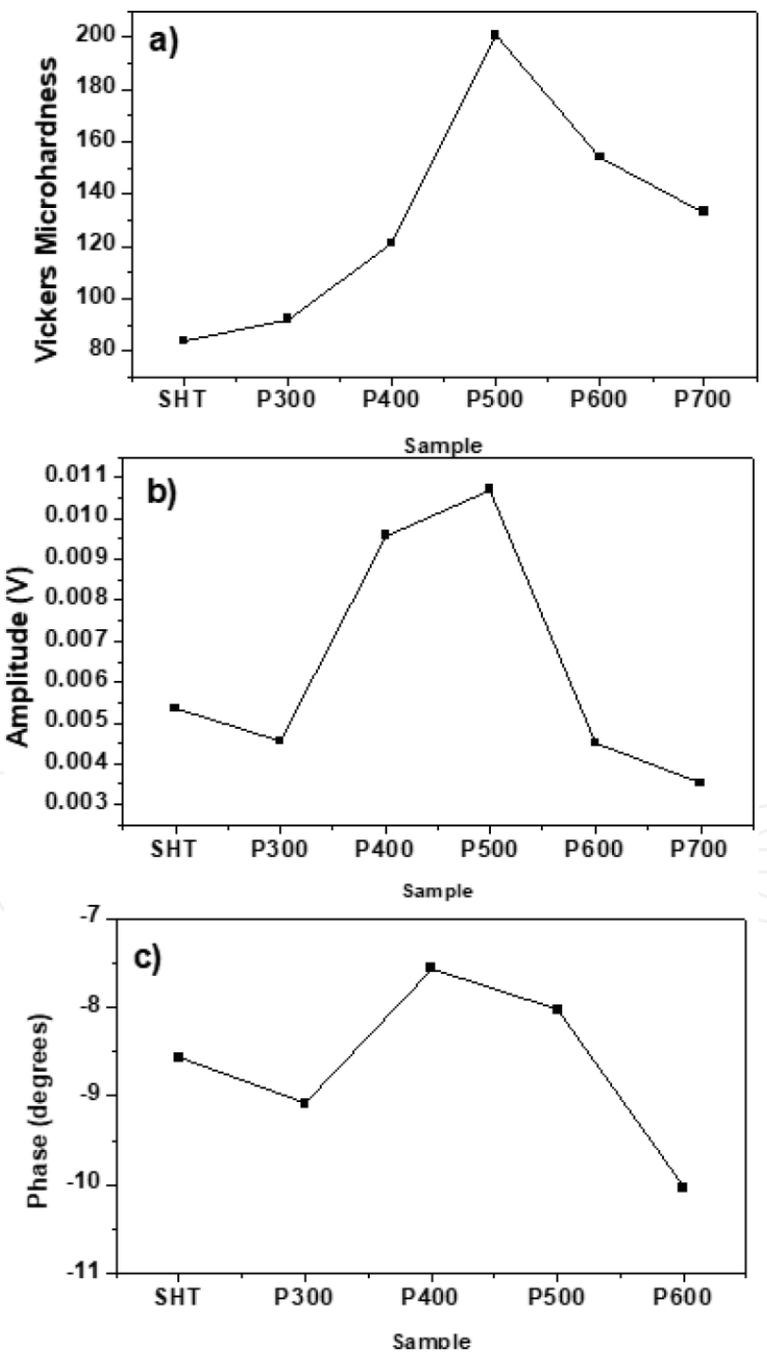

Figure 10.
Comparison among (a) Vickers microhardness and (b) amplitude and (c) phase signals of PTR applied to brass samples.

Multiphysics platform, is a basic approach to the application of the law of Lambert–Beer applied to the phenomenon of the absorption of laser light in a material. Due to the multiphysics profile of the program, it is possible to complement the model with other modules of the platform as geometrical optical to modified characteristics of laser beam incident in the material.

In the program it is considered that the definition of the mesh is one of the key points to obtain a good simulation that its erroneous choice the design of the same can cost the execution time of the program, or in the worst of the cases a bad convergence, translated into erroneous results.

The phenomenon of light absorption influences materials differently, depending on their physical–chemical properties such as thermal diffusivity, density, conductivity, and heat capacity. In the experimental results shown, it can be seen that the thermal treatments that involve the absorption phenomenon induce changes in the mechanical properties of the materials, such as microhardness. As reported in the Kunial brass samples analyzed, the PHT affected its metallurgical, thermal, and mechanical properties.

A marked correlation was found between the FWHM and the diffusivity. The diffusivity increased as the FWHM-1 increased. The highest diffusivity corresponds to 700°C while the lowest to the SHT sample.

The PTR amplitude signal was more sensitive than the PTR phase signal to observe the effect of the PHT temperature on alpha brass thermal, structural, and Vickers microhardness properties.

It is clear that the theoretical results obtained in COMSOL describe temperature variations as a function of the penetration depth of the incident radiation in the material, which in turn depends on factors such as the incident power. Because in the photothermal radiometry technique the thermal wave captured by the detector is translated as amplitude and phase signals, it is not possible to correlate both results. However, it is clear that a finite element analysis such as that offered by COMSOL offers the advantage of inferring the behavior of the variables involved in the process.

Among the possible improvements to the program are the inclusions of the modulation of the light source, which is a very important factor in the photothermal radiometry technique (PTR). The thermal wave generated in the material is very weak and necessarily requires an amplification. Without the modulation of the light source, the amplitude and phase parameters describing the thermal wave would not be possible to capture due to the amount of interference present in the medium. It is important to mention that the modulation frequency of the incident beam directly influences the penetration length in the material and consequently the propagation of the thermal wave.

With a more detailed theoretical–experimental analysis, it is possible to arrive at a comparable result between both parties, either by making measurements directly from temperature variations in the samples analyzed or by defining the variables and conditions in the program that allow obtaining the parameters of amplitude and phase of the generated thermal wave.

Acknowledgements

The authors thank Mario Enrique Rodríguez-Garcia of the Center of Applied Physics and Advanced Technology (CFATA, UNAM) for the support received for carrying out the experiments, the program Cátedras-CONACYT, and the National Council for Science and Technology (CONACyT) for funding through project 256923.

Author details

Minerva Robles-Agudo*, Martha Patricia Gonzalez-Tejeda,
Porfirio Esau Martinez-Muñoz and Ignacio Rojas-Rodríguez
CONACYT-Technological University of Querétaro (UTEQ), Querétaro, México

*Address all correspondence to: minerva.robles@uteq.edu.mx

References

[1] Copper Development Association. Brass in Focus 2004;177:1-4. Available from: http://copperalliance.org.uk/docs/librariesprovider5/resources/pub-177-brass-in-focus-pdf.pdf?Status = Master&sfvrsn = 0

[2] Khurmi RS, Gupta JK. A Textbook of Machine Design. 2004;**30**:6. Available from: https://es.slideshare.net/alianzam900/a-textbook-of-machine-design-by-rskhurmi-an-d-jkgupta-44120476

[3] Waheed A, Ridley N. Microstructure and wear of some high-tensile brasses. Journal of Materials Science. 1994;**29**:1692-1699. DOI: 10.1007/BF00368948

[4] Sadykov FA, Barykin NP, Aslanyan IR. Wear of copper and its alloys with submicrocrystalline structure. Wear Volumes. 1999;**225-229**:649-655. DOI: 10.1016/S0043-1648(98)00374-3

[5] Panagopoulos CN, Georgiou EP, Simeonidis K. Lubricated wear behavior of leaded α + β brass. Tribology International. 2012;**50**:1-5. DOI: 10.1016/j.triboint.2011.12.016

[6] Ozgowicz W, Kalinowska EO, Grzegorczyk B. The microstructure and mechanical properties of the alloy Cu-30%Zn after recrystallization annealing. Journal of Achievements in Materials and Manufacturing Engineering. 2010;**40**:15-25. Available from: http://jamme.acmsse.h2.pl/papers_vol40_1/4012.pdf

[7] Igelegbai EE, Alo OA, Adeodu AO, Daniyan IA. Evaluation of mechanical and microstructural properties of a α-brass alloy produced from scrap copper and zinc metal through sand casting process. Journal of Minerals and Materials Characterization and Engineering. 2017;**5**:18-30. Available from: https://file.scirp.org/pdf-JMMCE_2016122014370253.pdf. DOI: 10.4236/jmmce.2017.51002

[8] Bailey AR. The Structure and Strength of Metals, Annotated Metallographic Specimens. Betchworth: Gatwick Press Ltd.; 1967. pp. 75-88. Available from: http://www.worldcat.org/title/structure-and-strength-of-metals-an-elementary-practic-al-course-involving-th-correlation-of-microstructure-an-properties-in-32-specially-prepared-specimens/oclc/299573857

[9] Allmen MV, Blatter A. Laser-Beam Interactions with Materials, Physical Principles and Applications. 2nd ed. Springer; 1998. Available from: https://www.springer.com/gp/book/9783642970078

[10] COMSOL Multiphysics. Blogs. 2015. Available from: https://www.comsol.com/blogs/modeling-laser-material-interactions-with-the-beer-lambert-law/

[11] Buijs K, Maurice MJ. Some considerations on apparent deviations from Lambert-Beer's law. Analytica Chimica Acta. 1969;**47**(3):469-474. DOI: 10.1016/S0003-2670(01)95647-8

[12] Tolbin AY, Pushkarev VE, Tomilova LG. A mathematical analysis of deviations from linearity of Beer's law. Chemical Physics Letters. 2018;**706**(16):520-524. DOI: 1016/j.cplett.2018.06.056

[13] Casasanta G, Garra R. Towards a generalized Beer-Lambert law. Fractal and Fractional. 2018;**2**:8. DOI: 103390/FRACTALFRACT2010008

[14] Moosmüller H, Arnott WP. Particle optics in the Rayleigh regime. Journal of the Air and Waste Management Association. 2009;**59**:1028-1031. DOI: 10.3155/1047-3289.59.9.1028

[15] Uriarte LM, Bonales LJ, Dubessy J, Lobato A, Baonza VG, Cáceres M. The self-absorption phenomenon in quantitative Raman spectroscopy and how to correct its effects. Microchemical Journal. 2018;**139**:134-138. DOI: 10.1016/J.MICROC.201802.013

[16] COMSOL Multiphysics. Available from: https://www.comsol.com

[17] ASTM E92-82(2003) e2. Standard Test Method for Vickers Hardness of Metallic Materials, Subcommittee: E28.06, ASTM International; 2003. pp. 1-9

[18] Dias DT, Bedeschi VC, Ferreira da Silva A, Nakamura O, Castro-Meira MV, Trava-Airoldi VJ. Photoacoustic spectroscopy and thermal diffusivity measurement on hydrogenated amorphous carbon thin films deposited by plasma-enhanced chemical vapor deposition. Diamond and Related Materials. 2014;**48**:1-5. DOI: 10.1016/J.diamond.2014.06.003

[19] Rojas-Rodríguez I, Lara-Guevara A, Salazar-Sicacha M, Mosquera-Mosquera JC, Robles-Agudo M, Ramírez-Gutierrez C, et al. The influence of the precipitation heat treatment temperature on the metallurgical, microstructure, thermal properties and microhardness of an alpha brass. Materials Sciences and Applications. 2018;**9**:440-454. DOI: 10.4236/msa.2018.94030

[20] Lara-Guevara A, Rojas-Rodríguez I, Ortiz-Echeverri CJ, Robles-Agudo JM, Rodríguez-García ME. Thermal, structural, and microstructural characterization of eutectoid steel at different heat treatments. Journal of Materials Research. 2017;**32**:2202-2209. DOI: 10.1557/jmr.2017.47

[21] Lara-Guevara A, Ortiz-Echeverri CJ, Rojas-Rodriguez I, Mosquera-Mosquera JC, Ariza-Calderón H, Ayala-García I, et al. Microstructural, structural, and thermal characterization of annealed carbon. International Journal of Thermophysics. 2016;**37**(10):99. DOI: 10.1007/s10765-016-2105-6

[22] Demkó L, Kézsmárki I, Csontos M, Bordács S, Mihály G. Improved thermal relaxation method for the simultaneous measurement of the specific heat and thermal conductivity. European Physics Journal B. 2010;**74**:27-33. DOI: 10.1140/epjb/e2010-00055-0

[23] Rojas-Rodríguez I, Jaramillo-Vigueras D, Velázquez-Hernández R, Del Real A, Serrounkh I, Baños L, et al. Thermal and structural characterization of cooper-steel bonding interfaces produced by impact welding. Materials and Manufacturing Processes. 2008;**23**:823-828. DOI: 10.1080/10426910802384672

[24] Rosencwaig A, Gersho A. Theory of the photoacoustic effect with solids. Journal of Applied Physics. 1976;**47**: 64-69. DOI: 10.1063/1.322296

[25] Guo X, Sivagurunathan K, Garcia JA, Mandelis A, Giunta A, Milletari S. Laser photothermal radiometric instrumentation for fast in line industrial steel hardness inspection and case depth measurements. Applied Optics. 2009;**48**:11-22. DOI: 10.1364/AO.48.000C11